

## Evidence for strain compensation in stabilizing epitaxial growth of highly doped germanium

F. Tsui\* and L. He

*Department of Physics and Astronomy, University of North Carolina, Chapel Hill, North Carolina 27599, USA*

A. Tkachuk, S. Vogt, and Y. S. Chu

*Advanced Photon Source, Argonne National Laboratory, Argonne, Illinois 60439, USA*

(Received 9 October 2003; published 13 February 2004)

We report on a study of the epitaxial phase diagram of Co- and Mn-doped Ge(001) magnetic semiconductors. Complementary doping using dopants from different groups of elements can compensate for the effects of lattice strain caused by the doping species. Reducing lattice mismatch with the Ge host has been shown to be the key to stabilizing epitaxial growth and suppressing phase separation at higher doping levels. Applying this approach to other multidopant systems opens new prospects for tailoring highly doped electronic materials.

DOI: 10.1103/PhysRevB.69.081304

PACS number(s): 81.30.Dz, 81.15.Hi

One of the keys to the science and application of spintronics is our ability to control the electronic and magnetic properties of semiconductors by doping them with magnetic impurities during epitaxial growth.<sup>1,2</sup> The most desirable spintronic materials are semiconductors with room temperature ferromagnetism, and compatible with Si-based processing. Despite tremendous efforts in the field, particularly in Mn-doped materials,<sup>3,4</sup> no systems have come close to satisfying all of these conditions. The problem is that doping beyond several percent tends to induce too much epitaxial strain and to promote phase separation, thus making epitaxial growth unstable. The challenge, therefore, is how to stabilize relatively high levels of transition metal dopants required for achieving high temperature ferromagnetism without destroying the semiconductor. Complementary doping with several impurities has long been used to fine tune the electronic properties of semiconductors by adjusting the Fermi level with respect to the impurity levels.<sup>5</sup> However, its effects on structure and phase separation in highly doped materials synthesized from different groups of elements have not been examined systematically. Here we show that by using two transition metal dopants the strain effect in a group-IV element caused by the different species can be compensated for, thus stabilizing epitaxial growth and suppressing phase separation at higher doping levels. This is demonstrated in a Ge-based system doped with two commonly used transition metal elements, Co and Mn, where coherent epitaxial growth is stable within a narrow band of relative doping concentrations. Applying this approach to other multidopant systems opens new prospects for tailoring highly doped electronic materials.

The synthesis was carried out using advanced combinatorial molecular beam epitaxy techniques, in which the doping profile across each substrate can be tailored so that properties can be examined as a continuous function of thickness and composition during epitaxial growth.<sup>6</sup> This was accomplished by a combination of precision masks and sample manipulation, and real-time flux control using atomic absorption spectroscopy. Sequential doping of Co and Mn was employed at intervals of 2 Å of Ge, the “multilayer” method. The multicomponent nature of the work necessitated this approach. Typical samples are “binary,”

$\text{Co}_{ax}\text{Mn}_{bx}\text{Ge}_{1-x}$ , in which the total doping concentration  $x$  was varied with the relative concentration  $a/b$  being kept constant. Electron beam hearths were used for evaporating Ge and Co, and an effusion cell was used for Mn at a base pressure of  $10^{-11}$  torr. Ge(001) substrates were treated *in situ* through annealing-deposition cycles in order to produce atomically smooth surfaces for the study. The structural evolution and composition across the sample were examined using real-time scanning reflection high-energy electron diffraction (RHEED) imaging, and *ex situ* using microbeam (1–50 μm) x-ray diffraction (XRD) and x-ray fluorescence spectroscopy (XFS) with 10-keV incident x rays at XOR beamlines (2-BM, 7-ID-C, and 2-ID-E) of the Advanced Photon Source. Complementary experiments using *in situ* scanning probe microscopy (SPM) and cross-sectional high-resolution transmission electron microscopy (HRTEM) were also carried out.

At a temperature of 250 °C and a flux of  $\sim 0.1$  Å/s, the growth of lightly doped Ge(001) is layer by layer, similar to that for pure Ge(001) exhibiting two-dimensional (2D) RHEED patterns with  $2 \times 1$  surface reconstructions, as shown in Fig. 1(a), and RHEED oscillations. This persists up to a doping concentration  $x$ , above which a roughening transition occurs. Within a narrow range around the transition, and with vanishing 2D RHEED intensity and increasing peak width, 3D-like features appear [Fig. 1(b)]. At larger  $x$ , the RHEED patterns turn completely 3D, exhibiting modulated streaks and suppressed reconstruction patterns, as shown Fig. 1(c), and, as  $x$  increases further, the growth becomes increasingly disordered. Growth at temperatures below 200 °C and above 350 °C is generally disordered.

The presence of a composition-dependent roughening transition has been confirmed by XRD, SPM, and HRTEM measurements. These results also show that the films in the 2D regime are pseudomorphic, and that the roughening transition is accompanied by lattice relaxation and phase separation. As shown in Fig. 1(d), the x-ray scattering intensity in the 2D regime (black line) exhibits rapid oscillations that arise from the interference of the x-ray amplitudes scattered from the atomic layers of the substrate and the film, while the intensity from rough 3D growth (gray line) loses the simple periodicity.

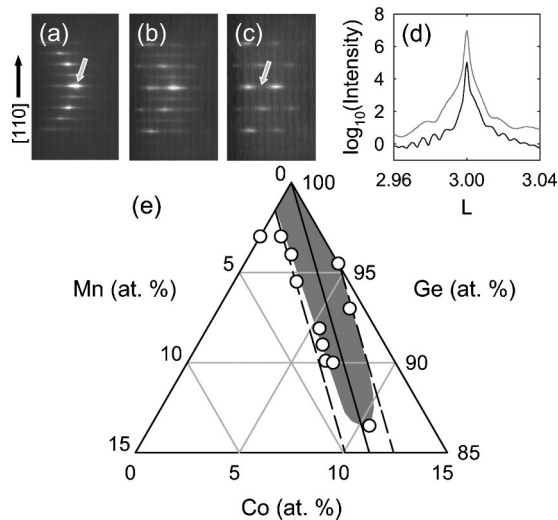


FIG. 1. Epitaxial phase diagram of Co- and Mn-doped Ge(001) films with thicknesses of 1000 Å. Distinct RHEED patterns along the [110] direction of Ge are shown in (a) for a 2D surface, (b) for a mixed 2D and 3D surface, and (c) for a 3D surface. To enhance the sensitivity for detecting the transition, the specular reflection, as indicated by the gray arrow in (a), was positioned at the “anti-Bragg” position between Bragg reflections, as indicated by the arrow in (c). (d) X-ray diffraction profiles along [11L] direction through Ge(113) reflection. The peak at  $L=3$  originates from the Ge substrate, while the oscillations are from the film-substrate interference. Black and gray lines correspond to 2D and 3D films, respectively. For clarity they are separated by a decade. (e) Roughening transition as a function of doping concentration (circles). The gray area indicates the region of smooth 2D epitaxial growth. The solid line indicates  $a/b \sim 3$ , where the intrinsic strains due to Co and Mn substitutional doping are fully compensated, while the dashed lines mark the boundary where the strain reaches  $\pm 0.07\%$ , as discussed in the text below [Eq. (1)].

From these measurements, an epitaxial phase diagram of the system has been determined, as shown in Fig. 1(e), where the observed transition is shown to depend sensitively on the relative doping concentration. Coherent 2D epitaxial growth occurs within a narrow window of composition (gray area) around  $a/b \sim 3$  (solid line) up to a combined maximum doping of  $\sim 14$  at.%. It is within this regime where promising Ge magnetic semiconductors were discovered with  $T_C$  approaching room temperature.<sup>7</sup> The 2D films are stable under post-growth annealing for temperatures up to 600 °C, above which phase separation occurs. Outside the 2D regime, films are rough, defective, and inhomogeneous. These observations, particularly the symmetry of the 2D regime in the phase diagram, suggest that lattice mismatch plays an important role. Since the tetrahedral radius of Co is smaller than that of Ge, while the Mn value is larger,<sup>8</sup> doping the two could compensate for the strain effects from each other within a range up to a critical value, as indicated by the dashed lines in Fig. 1(e).

To explore this, further XRD and XFS experiments have been carried out and analyzed. Samples with special doping profiles like the one shown in Fig. 2(a) were studied in order to separate the effects from the two dopants. As shown in

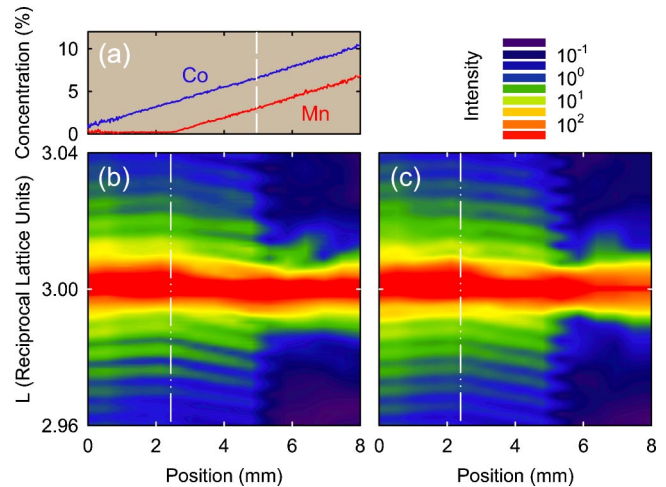


FIG. 2. (Color online) Composition and diffraction pattern of a Co- and Mn-doped Ge(001) sample with a thickness of 1000 Å. (a) Doping concentration of Co (blue) and Mn (red) vs the position on the sample as determined by XFS. (b) XRD intensity vs the reciprocal lattice vector  $L$  along the [11L] direction of Ge (vertical axis) and the position on the sample (horizontal axis). The position of the interference fringes for  $x < 5$  mm shifts linearly in  $L$ , centered at the dotted line. The fringes vanish above  $\sim 5$  mm [dashed line in (a)], indicating the transition to rough disordered growth with enhanced diffused scattering. (c) The corresponding fits of the XRD intensity using a simple kinematical model for positions  $< 5$  mm (Ref. 9), above which the behavior can no longer be fitted by a simple model. Instead, the latter was fitted using a more complex model with many parameters, which will be discussed elsewhere. As shown in the color chart [above (c)], the warmer color corresponds to a higher intensity, and for clarity the intensity is truncated at  $10^3$ .

Fig. 2(b) produced by a series of [11L] x-ray scattering profiles with the diffraction vector  $L$  along the growth direction, increasing Co doping causes the intensity oscillations (the interference fringes) to shift linearly toward higher values of  $L$ . In contrast, introducing Mn initiates a linear downward shift in  $L$  [to the right of dotted line in Fig. 2(b)]. The fringes disappear sharply at the roughening transition. This is accompanied by enhanced diffused scattering, indicating the onset of disorder. As mentioned above [Fig. 1(d)] the period of the oscillations gives a quantitative measure of the film thickness, while their phase along  $L$  is related to the strain between the film and substrate.

The diffraction patterns shown in Fig. 2(b) have been fitted using a simple kinematical model,<sup>9</sup> in which the number of atomic layers, the average atomic layer spacing, and the Debye-Waller factor were used as the fitting parameters. As shown in Fig. 2(c), this simple model produces satisfactory results, because the film thickness ( $1033 \pm 16$  Å, determined from the fitting and confirmed by HRTEM) is thin enough that the dynamical effects do not pose problems in determining the average strain of the film as a function of Co and Mn doping concentration. From this strain as a function of Co and Mn doping concentrations [Fig. 2(a)], has been determined. The result, as shown in Fig. 3 corrected for the tetragonal lattice distortion due to in-plane stress,<sup>10</sup> establishes that within the 2D regime the lattice spacing obeys Vegard’s

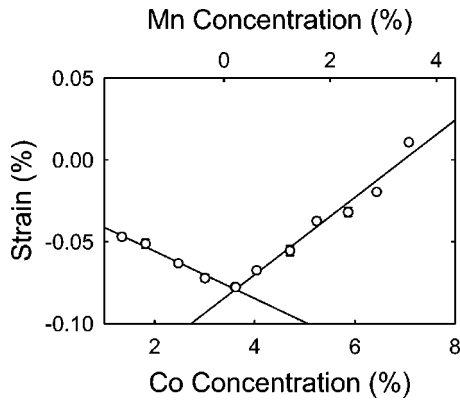


FIG. 3. Lattice mismatch between the doped Ge film and the Ge substrate as a function of Co and Mn doping concentration. The strain values were determined by fitting the diffraction patterns shown in Fig. 2(b) and corrected for the tetragonal distortion due to the in-plane stress (Ref. 10). The film thickness determined from the fits is  $1033 \pm 16$  Å.

law, such that the expansion due to Mn substitutional doping is compensated by the compression due to Co doping with the net strain  $\varepsilon$  given by

$$\varepsilon = -0.015ax + 0.045bx. \quad (1)$$

Here the two terms on the right hand side correspond to the effects from Co and Mn doping with the respective coefficients determined from XRD.<sup>11</sup> Tetrahedral covalent radii obtained from these values are 1.20 Å for Co and 1.27 Å for Mn using the Ge value of 1.22 Å, in excellent agreement with those from recent studies.<sup>8</sup>

Equation (1) establishes that at  $a/b \sim 3$  [solid line in Fig. 1(e)], the strain is fully compensated for, so the doped film is most stable. Here the transition may depend solely on the intrinsic energetics of phase separation, i.e., a chemical dependency. As  $a/b$  deviates from this value,  $|\varepsilon|$  increases and when it reaches a critical value  $\Delta$  [dashed lines in Fig. 1(e) with  $\Delta \sim 0.07\%$ ] and beyond, growth becomes unstable, i.e., a strain dependency, and surface roughening, lattice relaxation, and phase separation occur.

The evolution of the roughening transition as a function of film thickness provides a key insight into the underlying processes. As shown in Fig. 4, transitions near  $a/b \sim 3$  [along the solid line in Fig. 1(e)] and those away from it [across the dashed lines in Fig. 1(e)] exhibit qualitatively different thickness dependence with the latter [Fig. 4(b)] being much sharper than the former [Fig. 4(a)]. It is well known that lattice strain makes pseudomorphic growth unstable, thus giving rise to surface roughness and interfacial dislocations.<sup>12–15</sup> What is interesting, however, is the apparent coincidence of surface roughening, lattice relaxation, and phase separation. Quantitatively, the thickness at which the transition occurs,  $h_c$  for strain values of  $<0.1\%$  is much too small compared to those observed in similar systems,<sup>16,17</sup> even smaller than what is predicted by equilibrium theory.<sup>12–15</sup> Furthermore, the functional form for  $h_c$  exhibits a  $1/(\varepsilon - \varepsilon_0)$  strain dependence [or a  $1/(x - x_0)$  composition

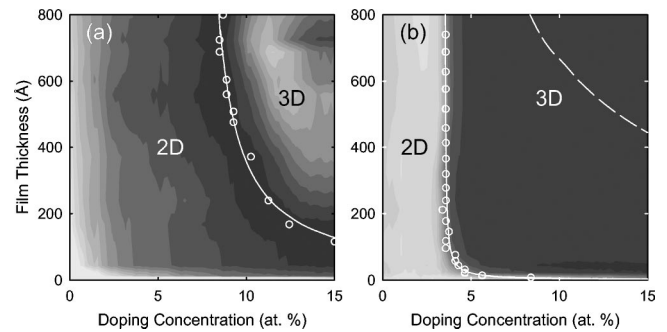


FIG. 4. Evolution of the roughening transition: RHEED intensity as a function of doping concentration and film thickness for samples (a)  $\text{Co}_{0.7x}\text{Mn}_{0.3x}\text{Ge}_{1-x}$  and (b)  $\text{Co}_x\text{Ge}_{1-x}$ . The 2D and 3D intensities correspond to integrated intensities of the specular reflection at the anti-Bragg position [the gray arrow in Fig. 1(a)] and a nearby Bragg reflection [the one to the right of the arrow in Fig. 1(c)], respectively. Circles indicate the crossover points in intensity between the 2D and 3D features, and lines correspond to fits using  $\alpha/(x - x_0)$  discussed in the text with respective  $\alpha$  and  $x_0$  values for (a)  $10 \pm 2$  Å and  $7.3 \pm 0.5\%$ , and for (b)  $0.32 \pm 0.04$  Å and  $3.5 \pm 0.4$ . The dashed line in (b) corresponds to the equilibrium prediction (Refs. 12 and 14) with the strain values calculated using Eq. (1), but a corresponding curve for (a) is out of the plot range.

dependence, as shown in the fits in Fig. 4 with constants  $\varepsilon_0$  and  $x_0$ ] rather than the predicted  $1/\varepsilon$  [also shown in the dashed line in Fig. 4(b)].<sup>12–15</sup> These findings suggest that phase separation in addition to strain may play a dominant role in determining the observed phenomenon.

The presence of a solubility gap that promotes the tendency toward phase separation even in the absence of strain gives rise to a solid mixture energy that may be parametrized by a second order polynomial in concentration  $x$ ,<sup>18</sup> whose area density is proportional to thickness  $h$ . The energy cost for the system to remain in solid solution can be balanced by the energy associated with generation of interfacial defects, which generally depends on  $x$  but not on  $h$ .<sup>12–15</sup> The two energies are comparable at  $h_c$ , where generation of interfacial defects becomes viable and thus homogeneous epitaxial growth becomes unstable. This leads to the functional form described above, with a characteristic cutoff  $x_0$  from the linear term in  $x$  in the mixing energy. The presence of strain would further reduce the stability of the epitaxial growth, since the strain energy depends on  $\varepsilon^2$  [or  $x^2$  using Eq. (1)] and  $h$ , but it will not change the functional form. Instead, it will make the concentration dependence of  $h_c$  sharper, owing to the reduced proportionally constant and  $x_0$ , as shown in Fig. 4.

While the two-phase parametrization discussed here for the thermodynamics is probably oversimplified, the importance of interfacial defect generation in controlling the observed transition is quite evident. Defect-free pseudomorphic growth, with the lattice strain fully compensated for, resists phase separation, but defective growth and the presence of lattice mismatch would trigger an earlier onset of disorder and inhomogeneity.

In summary, the epitaxial phase diagram of Co and Mn doped Ge(001) films has been studied. Complementary doping using dopants from different groups of elements to compensate for the effects of lattice strain has been shown to be the key for stabilizing epitaxial growth at higher doping levels. This approach of complementary doping using known properties can dramatically enhance the search for desirable electronic materials by reducing the number of potential

candidates, especially when both lattice and electronic compensations among the doping species are present.

The authors thank D. Walko and P. Ilinski at APS for experimental assistance. The work was supported in part by the U.S. National Science Foundation, Grant No. DMR-0108605. Use of the Advanced Photon Source was supported by the U.S. Department of Energy, Office of Science Basic Energy Sciences, under Contract No. W-31-109-ENG-38.

\*Electronic address: ftsui@physics.unc.edu

<sup>1</sup>G. A. Prinz, *Phys. Today* **48** (4), 58 (1995).

<sup>2</sup>S. A. Wolf, D. D. Awschalom, R. A. Buhrman, J. M. Daughton, S. von Molnar, M. L. Roukes, A. Y. Chtchelkanova, and D. M. Treger, *Science* **294**, 1488 (2001).

<sup>3</sup>H. Ohno, *Science* **281**, 951 (1998).

<sup>4</sup>Y. D. Park, A. T. Hanbicki, S. C. Erwin, C. S. Hellberg, J. M. Sullivan, J. E. Mattson, T. F. Ambrose, A. Wilson, G. Spanos, and B. T. Jonker, *Science* **295**, 651 (2002).

<sup>5</sup>E. H. Putley, *The Hall Effect and Semiconductor Physics* (Butterworth, London, 1960), Chap. 5.

<sup>6</sup>Y. K. Yoo and F. Tsui, *MRS Bull.* **27**, 316 (2002).

<sup>7</sup>F. Tsui, L. He, L. Ma, A. Tkachuk, Y. S. Chu, K. Nakajima, and T. Chikyow, *Phys. Rev. Lett.* **91**, 177203 (2003).

<sup>8</sup>R. K. Iwanowski, Lawniczak-Jablonska, Z. A. Golacki, and K. Traverse, *Chem. Phys. Lett.* **283**, 313 (1998).

<sup>9</sup>I. K. Robinson, *Rep. Prog. Phys.* **55**, 599 (1992).

<sup>10</sup>The correction factor for the tetragonal distortion is  $(1 + \nu)/(1 - \nu)$  for the (001) system, with a Poisson ratio  $\nu$  of 0.27 for Ge.

<sup>11</sup>There is a 25% uncertainty associated with these coefficients from the systematic errors in the composition measurements.

<sup>12</sup>J. H. Van der Merwe and C. A. B. Ball, in *Epitaxial Growth*, edited by J. W. Matthews (Academic, New York, 1975), Pt. B, Chap. 6.

<sup>13</sup>J. W. Matthews and A. E. Blakeslee, *J. Cryst. Growth* **27**, 118 (1974); **29**, 273 (1974).

<sup>14</sup>R. People and J. C. Bean, *Appl. Phys. Lett.* **47**, 322 (1985).

<sup>15</sup>R. C. Cammarata, *Prog. Surf. Sci.* **46**, 1 (1994).

<sup>16</sup>J. C. Bean, L. C. Feldman, A. T. Fiory, S. Nakahara, and I. K. Robinson, *J. Vac. Sci. Technol. A* **2**, 436 (1984).

<sup>17</sup>P. J. Orders and B. F. Usher, *Appl. Phys. Lett.* **50**, 980 (1987).

<sup>18</sup>C. Kittel and H. Kroemer, *Thermal Physics* (Freeman, San Francisco, 1980), Chap. 11.